

NRC Publications Archive Archives des publications du CNRC

Nanoplastic reference materials for biological and methodological assessment

Pegoraro, Adrian F.; Chen, Maohui; Sakib, Sadman; Jakubek, Zygmunt J.; Maan, Zeina; Prezgot, Daniel; Sallam, Aliya; Corriveau, David; Vandenberg, Magda; Zou, Shan

This publication could be one of several versions: author's original, accepted manuscript or the publisher's version. / La version de cette publication peut être l'une des suivantes : la version prépublication de l'auteur, la version acceptée du manuscrit ou la version de l'éditeur.

For the publisher's version, please access the DOI link below. / Pour consulter la version de l'éditeur, utilisez le lien DOI ci-dessous.

Publisher's version / Version de l'éditeur:

<https://doi.org/10.1186/s43591-025-00157-2>

Microplastics and Nanoplastics, 6, 1, pp. 1-18, 2025-12-01

NRC Publications Archive Record / Notice des Archives des publications du CNRC :

<https://nrc-publications.canada.ca/eng/view/object/?id=7c91e212-0a2c-4153-bb63-9be8cefe4394>

<https://publications-cnrc.canada.ca/fra/voir/objet/?id=7c91e212-0a2c-4153-bb63-9be8cefe4394>

Access and use of this website and the material on it are subject to the Terms and Conditions set forth at

<https://nrc-publications.canada.ca/eng/copyright>

READ THESE TERMS AND CONDITIONS CAREFULLY BEFORE USING THIS WEBSITE.

L'accès à ce site Web et l'utilisation de son contenu sont assujettis aux conditions présentées dans le site

<https://publications-cnrc.canada.ca/fra/droits>

LISEZ CES CONDITIONS ATTENTIVEMENT AVANT D'UTILISER CE SITE WEB.

Questions? Contact the NRC Publications Archive team at

PublicationsArchive-ArchivesPublications@nrc-cnrc.gc.ca. If you wish to email the authors directly, please see the first page of the publication for their contact information.

Vous avez des questions? Nous pouvons vous aider. Pour communiquer directement avec un auteur, consultez la première page de la revue dans laquelle son article a été publié afin de trouver ses coordonnées. Si vous n'arrivez pas à les repérer, communiquez avec nous à PublicationsArchive-ArchivesPublications@nrc-cnrc.gc.ca.

RESEARCH

Open Access



Nanoplastic reference materials for biological and methodological assessment

Adrian F. Pegoraro^{1*}, Maohui Chen¹, Sadman Sakib¹, Zygmunt J. Jakubek¹, Zeina Maan¹, Daniel Prezgot¹, Aliya Sallam¹, David Corriveau¹, Magda Vandenberg¹ and Shan Zou^{1*}

Abstract

Plastic particles are pervasive across all environments, yet quantifying their total abundance remains challenging—especially for nanoplastics, which are problematic to separate and detect efficiently. This challenge is further exacerbated by the heterogeneous nature of environmental nanoplastics, making it difficult to determine their biological impacts. Despite these limitations, correlational studies implicate that nanoplastics may pose potential health concerns for both wildlife and humans. Metrological reference materials can be used to address this gap; these standardized plastics enable validation of detection technologies and support biological investigations. One such material has recently been made available (NPPP-1, National Research Council of Canada) with more to follow in the future. These materials are produced using ultrashort laser pulses for laser ablation, a versatile approach for the high-throughput production of nanoplastics. The resulting nanoplastics resemble those found in the environment, exhibiting heterogeneous sizes and shapes, as well as modified chemical fingerprints associated with environmental weathering, while remaining stable in different media, allowing their use in biological and ecotoxicology testing. In both two-dimensional cell culture and three-dimensional organoid models, nanoplastics are shown to have limited effects on cell viability at relatively high number concentrations while activating inflammatory pathways in biological systems. Taken together, it is demonstrated that nanoscale plastics produced using ultrashort laser ablation are fit for purpose for both validating quantification methods and assessing biological activity.

Keywords Nanoplastics, Laser ablation, Reference materials, Nanotoxicity, Nanometrology

Introduction

Plastic pollution is a growing global health concern, with micro- and nanoplastics (MNPs) detected in every environment on the planet, as well as in many living creatures [1–3]. Human exposure to MNPs can occur through water, food and even air. While some MNPs are primary

in nature, that is, they are specifically manufactured at that size, a key source of MNPs is the fragmentation and weathering of macroplastics in the environment through abrasion, exposure to UV radiation and biological degradation [4–8]. These weathered materials become heterogeneous in terms of size, surface chemistry, and distribution, making it challenging to classify them and determine their biological impacts [9–12]. This is further complicated when considering the association of MNPs with other chemicals, such as heavy metals, which can alter their potential toxicity and behavior in the environment [13, 14]. To address the challenge of detecting and classifying MNPs, substantial efforts have been

*Correspondence:

Adrian F. Pegoraro
adrian.pegoraro@nrc-cnrc.gc.ca

Shan Zou
shan.zou@nrc-cnrc.gc.ca

¹Metrology Research Centre, National Research Council of Canada, 100
Sussex Dr, Ottawa, ON K1A 0R6, Canada



© Crown 2025. **Open Access** This article is licensed under a Creative Commons Attribution 4.0 International License, which permits use, sharing, adaptation, distribution and reproduction in any medium or format, as long as you give appropriate credit to the original author(s) and the source, provide a link to the Creative Commons licence, and indicate if changes were made. The images or other third party material in this article are included in the article's Creative Commons licence, unless indicated otherwise in a credit line to the material. If material is not included in the article's Creative Commons licence and your intended use is not permitted by statutory regulation or exceeds the permitted use, you will need to obtain permission directly from the copyright holder. To view a copy of this licence, visit <http://creativecommons.org/licenses/by/4.0/>.

made to develop tools for identifying MNPs in different environments [15–17]. The detection and classification of nanoplastics is a particularly pressing problem, given that they can cross biological barriers and enter cells and tissues [18–20]. While there is agreement that nanoplastics pose a societal concern [21, 22], there remain challenges in determining how they should be regulated. As an example, there is a lack of clarity on how to classify nanoplastics as a subset of MNPs [23–27]. Many regulatory bodies classify nanoscale materials as having at least one dimension in the 1–100 nm size range [28, 29]. However, for concerns regarding human health, this upper bound can be extended to 1000 nm [29]. For this and other reasons, many argue that nanoplastics should be defined as 1–1000 nm in size even if that falls outside the defined range of nanoscale materials [23, 30]. Beyond concerns regarding classification, there are also methodological challenges in quantifying nanoplastic content and its biological impact, hindering regulatory development [31–33].

One method of addressing these concerns is the development of model nanoplastics, which reproduce the properties of plastic found in the environment and can be used as reference materials (RMs). These materials should be sufficiently homogenous and stable for detection limit determination of different techniques, allow for the validation of measurement methods and enable independent evaluation of the health effects of nanoplastics on living organisms [4–6]. Ideally, such materials will capture key properties of plastics found in the environment: heterogeneous in size, varied in shape, altered chemistry due to weathering and derived from macroplastics. Furthermore, for use in biological testing, these materials should be stable in a range of solutions and free of other potential contaminants such as surfactants, adhered pollutants or additives, which can leach out of the plastics. Finally, these materials should be available in sufficient quantity to allow for repeated experimentation across different organisms and detection technologies so that results can be independently validated. Several efforts have been made previously to address this issue [4–6]. For example, different studies have synthesized nanoparticles for batch fabrication [34–38]; however, the relative homogeneity of the final product and the presence of surfactants in some approaches make it unclear if these materials will mimic the biological effects of environmental plastics [39]. Several simulated weathering approaches have also been used as an alternative to synthesis [5, 40, 41]. Mechanical degradation using processors/blenders and cryo-milling can be employed to fabricate nanoplastics [42–46] in limited quantities at small particle sizes or batch quantities at larger particle sizes; however, contamination from the metals used may be a concern. Accelerated aging using UV exposure, heat, sonication, or a combination

of those techniques also produces sub-micron plastics [40, 41, 47–49]; however, it cannot reach the smallest size ranges of nanoplastics or produce scalable quantities. Laser ablation using high-energy UV pulsed lasers generates a wide range of particle sizes when the material is simultaneously ionized and melted; these materials can be subsequently filtered to recover nanoplastics [50, 51]. This type of laser ablation can result in a significant heat affected zone and thermal alteration to the surface, limiting the ability to produce particles continuously without constantly renewing the sample, presenting challenges for high throughput production. Additionally, the UV laser can be absorbed by the nanoparticles in solution, potentially leading to subsequent degradation of the material. A lack of reliable nanoplastic RMs remains, hindering researchers' widespread access to validate detection technologies and assess the biological effects of nanoplastic exposure.

Here, we demonstrate a new technique for the fabrication of nanoplastics from different macroplastics, which produces large quantities of stable, reproducible particles that allow us to test the effects of nanoscale plastic exposure on biological systems. To generate nanoplastics, we utilize an ultrashort laser to perform cold ablation on a bulk plastic, which deposits minimal heat into the sample and thus does not substantially melt the underlying material [52–54]. This approach is remarkably flexible, allowing for the fabrication of different nanoplastics from a range of plastic source materials without changes to the overall setup. We demonstrate the production of nanoscale polypropylene (PP), high-density polyethylene (HDPE) and polyethylene terephthalate (PET), demonstrating the versatility of this approach. We find that the produced material is heterogeneous in size and shape distribution, spanning a range from a few nanometers to 100s of nm. The produced particles exhibit chemical alterations, including oxidation patterns similar to those observed in weathered environmental plastics. Importantly, we find that the materials are stable in water and cell media, allowing their use in biological screening. To evaluate the applicability of laser ablated nanoplastics in biological assays and to examine their potential cellular and organoids responses, we exposed cultured cells and model organoids to these materials. The results indicate pro-inflammatory responses and apoptosis at high concentrations. The nanoscale PP described here is available to others as an RM [55] with the HDPE and PET to be made available in the future.

Results

Fabrication

Laser ablation of dielectrics using femtosecond lasers typically proceeds via multiphoton ionization [52–54]. Here, we use a 1030 nm, 200 fs laser with an average

power of 1.4 W, operating at a repetition rate of 200 kHz. The laser is focused to a diameter of approximately 25 μm , giving a peak intensity at the focus of $\sim 7 \text{ TW}/\text{cm}^2$ (see Fig. 1a and Methods for additional details). Because multiphoton processes only occur at regions of high instantaneous intensity, ablation and material modification are largely confined to the focal volume in all three dimensions. Material is only removed within the focal volume and by raster scanning the focus, it is possible to continuously remove new material. The long wavelength used here is not directly absorbed by the material being ablated. Taken together, these effects substantially reduce the heat deposited into the material, reducing the heat affected zone of the laser [52–54]. This is in contrast to laser ablation using nanosecond lasers where an extensive heat affected zone can be generated and the surrounding

material significantly modified in terms of its structural and chemical properties. We note that in plastics that have lower band gaps, that are nonetheless far from the linear absorption regime, the rate of material removal can be markedly higher. To increase throughput and further reduce the effects of potential heat damage, the laser is scanned continuously during ablation with a 50% overlap between subsequent laser pulses. To facilitate large-batch collection, the sample is translated along the focal axis, allowing new material to be continuously exposed to the ablation process. The material was typically ablated over the course of 72 h, with all particles collected into 500 mL of continuously circulating milli-Q water using a peristaltic pump. After 72 h, the rate of ablation slowed, likely due to the high concentration of nanoplastics in the circulating water, which can alter the focusing conditions

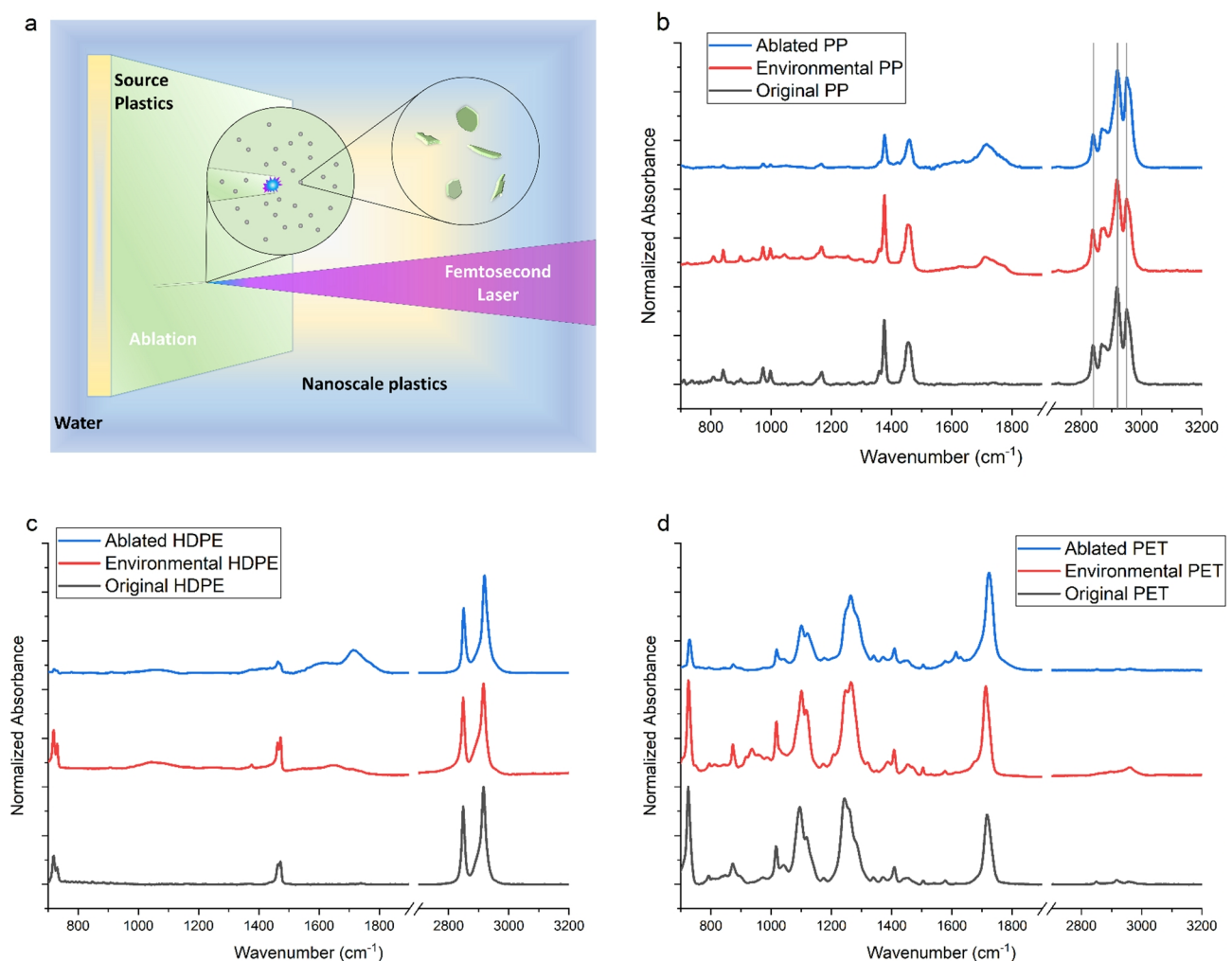


Fig. 1 Nanoplastic fabrication and chemical characterization. **(a)** Nanoplastics are formed using cold-ablation with a femtosecond laser. The laser is raster-scanned across the surface and material collected into water. **(b)** Comparison of IR spectrum of PP samples from original source material (black), spectrum from FLOPP-e database (red) and laser ablated material (blue) For ease of comparison, the bands at 2840 cm^{-1} , 2920 cm^{-1} , and 2950 cm^{-1} have been identified with vertical lines. **(c)** Comparison of IR spectrum of HDPE samples from original source material (black), spectrum from FLOPP-e database (red) and laser ablated material (blue) **(d)** Comparison of IR spectrum of PET samples from original source material (black), spectrum from FLOPP-e database (red) and laser ablated material (blue)

of the laser. Given ablation is confined to only the focal volume of the laser, we do not expect that the circulating plastics in solution are degraded by passing the infrared beam. After ablation, the solution was filtered using a 2.7 μm glass microfiber filter and stored in a glass container at (2 to 5) $^{\circ}\text{C}$. Under these conditions, it was possible to fabricate the plastics required for the physical, chemical and biological experiments reported here in approximately 1 week with a yield of ~ 60 mg of nanoscale plastic per week [55].

Chemical characterization

As plastic weathers in the environment, it can undergo chemical changes, with an increase in oxidation being a notable alteration [47, 56]. Previous efforts using UV laser ablation have demonstrated the presence of oxygen-rich groups on the surface of the particles after ablation [50]. To assess whether the nanoplastics produced here demonstrate similar shifts in chemical signature while remaining identifiable as plastic, we use infrared (IR) spectroscopy and microscopy. Attenuated total reflectance (ATR) Fourier transform infrared (FTIR) spectroscopy was used to measure IR absorption spectra of bulk plastic pre-laser ablation. Additionally, we used transmission FTIR spectroscopy of films of nanoplastic particles deposited onto silicon substrates. As a point of comparison, we used environmental FTIR spectra from the FLOPP-e database as a reference weathered spectrum for each material [57]. In all cases, we see evidence that weathering and laser ablation alter the chemical signature of the plastics formed, as shown in Fig. 1b-d. Specifically, we find evidence of increased oxidation and bond breaking. For example, when comparing the bulk unmodified PP samples to the laser-ablated and weathered PP (“PP1” in the FLOPP-e database [57]), we find that while the main characteristic chemical signatures of PP remain, there is a relative decrease in strength of the IR peaks at 2840 cm^{-1} and 2920 cm^{-1} , which are associated with CH_2 groups when compared to the mode at 2950 cm^{-1} associated with CH_3 groups. Additionally, we note the appearance of a new peak centered around 1725 cm^{-1} (see Fig. 1b). These changes are consistent with bond breaking due to ionization and the formation of carbonyl groups during oxidation; interestingly, the peak at 1725 cm^{-1} has been previously used to estimate the degree of weathering in environmental samples [58, 59]. It is notable that the carbonyl peak is strongest for the generated nanoplastics; given that previous reports have suggested carbonyl groups can form on the surface of the nanoplastics [50], these results are consistent with a substantial increase in surface area of the plastics generated.

We also find evidence of oxidation in the IR spectrum of HDPE, with both laser ablated and weathered material (“PE1” in the FLOPP-e database [57]) having a peak

around 1725 cm^{-1} , which is absent in the pristine sample (see Fig. 1c). Without a strong independent signal from CH_3 groups at 2950 cm^{-1} , it is not possible to measure the relative change in the strength of the peaks associated with CH_2 groups in the processed HDPE samples versus the pristine ones. Nonetheless, there is a variation across the samples in the relative strength of the 2850 cm^{-1} peak compared to the peak at 2920 cm^{-1} . We find that in the weathered samples, the 2850 cm^{-1} peak is stronger, whereas it decreases with laser ablation compared to the untreated sample. Given the weathered material was waste and has an unknown origin, it is possible that this difference could be due to the initial formulation of the material.

The evidence of oxidation in the laser-ablated PET samples is more ambiguous than for PP and HDPE, given that PET has carbonyl moieties as initially formulated; this is consistent with previous research, which has noted there are relatively minor changes in the FTIR spectrum of weathered PET unless a high degree aging has occurred [60–62]. Nonetheless, it is possible to compare relative changes across the spectrum (Fig. 1d). Note that we have used an environmental FTIR spectrum, “PET22” from the FLOPP-e database as a reference [57]. We find the peaks at 1100 cm^{-1} and 1245 cm^{-1} , corresponding to aromatic ester stretches, appear to be less altered during ablation compared to the CH_2 peak at 735 cm^{-1} , which decreases. We also observe that the carbonyl peak at 1725 cm^{-1} broadens, a change which has previously been associated with aging in PET [62]. These changes are consistent with those observed for PP and with previous findings on PET nanoplastics [50], suggesting the formation of carbonyl groups on the surface of nanoplastics during oxidation.

Physical morphology characterization

With the chemical identity of the different nanoplastics confirmed to be preserved during the laser ablation process, we characterized the particle size distributions (PSDs). For nanoparticles, numerous sizing techniques are available, offering complementary information about the samples. While different techniques yield consistent size results for monodispersed samples, polydispersity can present challenges when attempting to determine the PSD and number concentration of nanoparticle dispersions [63–67]. To better characterize the size and shape of the particles, we employed a multimodal approach using dynamic light scattering (DLS), nanoparticle tracking analysis (NTA) and atomic force microscopy (AFM). Both light scattering techniques (DLS and NTA) show a decreased detection efficiency for the smallest particles in polydisperse samples due to differential scattering cross-sections, which makes it challenging to fully determine the PSD. For AFM, accurately measuring particle

concentration and determining stability in different dispersions is challenging. Only by comparing and contrasting the different techniques can we characterize samples with a high degree of polydispersity.

As anticipated, the intensity-weighted PSD recorded using DLS exhibits evidence of substantial polydispersity (see Fig. 2a for PP, for HDPE and PET, see Supporting Figure S1a and S2a). For example, the PP sample displays a single peak with a mean particle diameter of (269 ± 12) nm and a distribution standard deviation of (162 ± 17) nm, indicating a broad size range. Similarly, the mean particle diameter and distribution standard deviation are (260 ± 21) nm and (159 ± 35) nm for HDPE, and (217 ± 32) nm and (108 ± 19) nm for PET. These results confirm that the short pulse laser-generated plastics are nanoscale and heterogeneous in lateral size, as desired for use as an RM modeling environmental plastic.

The high degree of polydispersity makes it challenging to directly convert DLS generated intensity-weighted PSDs to number-weighted PSDs, especially if the shape factor is unknown [67]. To mitigate this difficulty, the dispersions were also analyzed using NTA, which provides a number-weighted PSD and complementary information on number concentration. Analyses were performed on a dilution series to enable efficient detection of small particles in the presence of larger ones. Dilution-corrected concentrations were observed to vary with dilution (see Supporting Figure S3); for estimating doses in biological

experiments, concentrations were determined at dilutions corresponding to approximately 10 particles/frame, which is the lower limit of the range recommended by the instrument manufacturer. At these conditions, particle concentrations after laser ablation and without further concentration processing were measured as $(6.3 \pm 2.1) \times 10^{10}$ particles/mL for PP, $(3.2 \pm 0.7) \times 10^{10}$ particles/mL for HDPE, and $(4.3 \pm 1.0) \times 10^{10}$ particles/mL for PET. Importantly, as dilution increased and the number of detected particles decreased, the measured particle size remained consistent, provided the particle count per frame was within the instrument's specified range of (10 to 100) particles/frame.

Using NTA, the average number-weighted particle diameters were (105 ± 15) nm for PP, (115 ± 18) nm for HDPE, and (126 ± 24) nm for PET. The smaller sizes compared to DLS are expected, as intensity-weighted PSDs are biased toward larger particles. Indeed, if we perform a simple conversion of the DLS-generated intensity-weighted PSD to a number-weighted PSD, ignoring the challenges of polydispersity and assuming a spherical particle shape, we find that the number-based PSDs measured using DLS and NTA agree satisfactorily well (see Fig. 2b for PP data, Supporting Figure S1b for HDPE, Supporting Figure S2b for PET).

In the DLS number-weighted distribution of PP (see Fig. 2b), a shoulder is observed below 50 nm. For both DLS and NTA, we expect that the smallest particles are

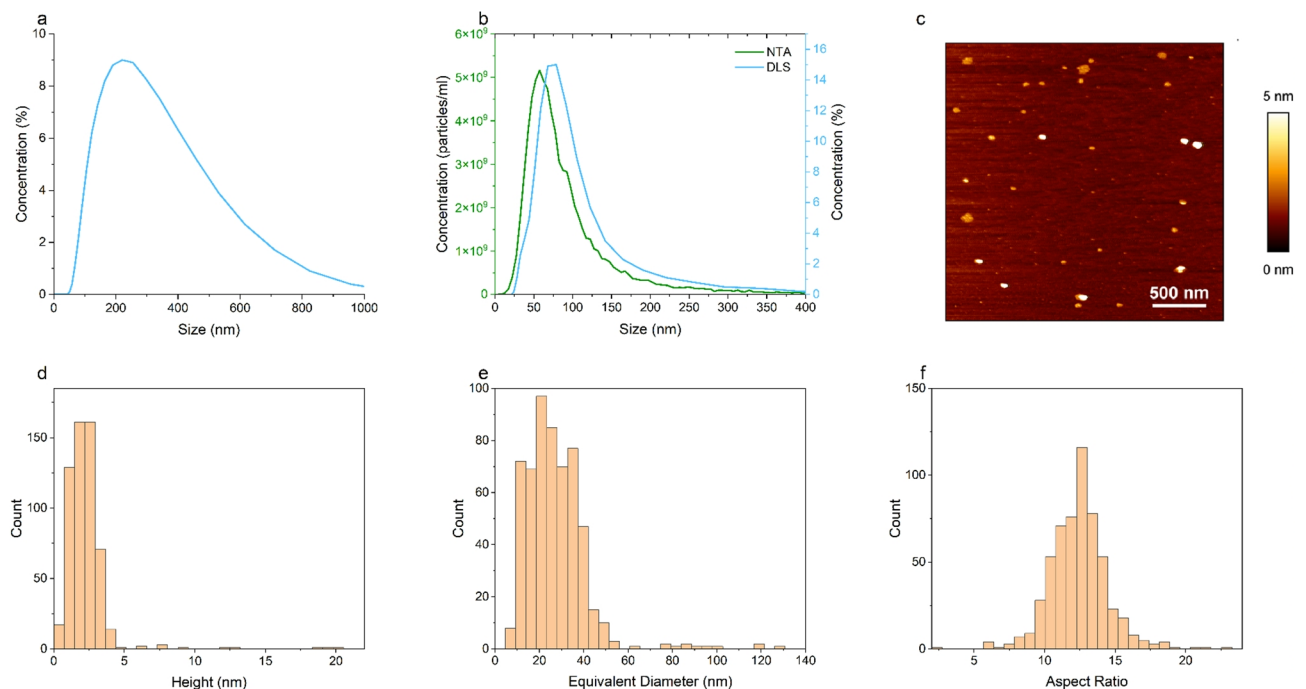


Fig. 2 Physical characterization of PP nanoplastics. **(a)** intensity-weighted PSD measured using DLS **(b)** number-weighted PSD measured using NTA (left axis) and DLS (right axis). NTA distribution has been corrected for dilution. **(c)** Representative AFM image of PP nanoplastics **(d)** Height distribution of PP nanoplastics characterized using AFM **(e)** Equivalent diameter distribution of PP nanoplastics characterized using AFM **(f)** Aspect ratio of PP nanoplastics. Aspect ratio taken as diameter/height. Equivalent data for HDPE and PET can be found in the SI

undercounted due to the limited dynamic range in the instruments. To examine these smallest particles and assess the shapes of the nanoplastics' particles, AFM was used to record the three-dimensional morphology of the particles, with a specific focus on the smallest objects that light scattering techniques may miss (see Fig. 2c, Supporting Figure S1c, Supporting Figure S2c, for detailed measurement protocol, see Methods). Here, we illustrate the results with PP fabricated nanoplastics (Fig. 2d-f); results for HDPE and PET can be found in the SI (Supporting Figure S1, S2). The particles have irregular shapes and span a wide size range. Given the discoidal morphology of the smaller particles, the circle-equivalent diameter—defined as the diameter of a circle with the same projected area—was used for size characterization. Both the particle height (Fig. 2d) and equivalent diameter (Fig. 2e) distributions are skewed with long tails at higher values. The mean heights and the standard deviation of the height distributions are (2.2 nm, 1.7 nm) for PP, (17 nm, 16 nm) for HDPE, and (13 nm, 10 nm) for PET, respectively. The corresponding mean circle-equivalent diameters and the standard deviation of the diameter distributions of PP, HDPE, and PET are (27 nm, 14 nm), (34 nm, 27 nm), and (32 nm, 22 nm), respectively. These results are consistent with fragmentation and weathering processes, which typically produce asymmetric particles with broad size distributions.

Based on the discoidal morphology, aspect ratios (diameter/height) were also calculated (PP: Fig. 2f, HDPE: Supporting Figure S1f, PET: Supporting Figure S2f). The mean aspect ratios and standard deviations are (12.4, 2.1) for PP, (2.1, 0.8) for HDPE, and (2.5, 1.0) for PET. This observation supports the interpretation of the strong carbonyl signals observed via IR spectroscopy as surface-related features; the enhanced surface-to-volume ratio of the nanoplastics likely contributes to the prominence of these chemical signatures.

Stability characterization

For use in biological systems and as an RM, nanoscale plastics must be long-term stable against aggregation and agglomeration. While this can be achieved with surfactants and stabilizers, we do not add any exogenous agents to the dispersions here because those additives are unlikely to be present in environmental plastics and may themselves provoke a biological response [39]. Despite this, we observe them to remain long-term stable. To better understand the underlying mechanism of stability, we measure the zeta-potential of the nanoplastic dispersions in water. We find that the mean zeta-potential and zeta deviation (standard deviation of the distribution) values respectively are (-51.7 ± 1.7) mV and (6.3 ± 0.6) mV for PP, (-46.9 ± 3.9) mV and (6.8 ± 1.5) mV for HDPE, and (-42.2 ± 0.7) mV and (8.0 ± 0.4) mV for PET, indicating

highly stable suspensions. This indicated that the plastic nanoparticles would likely also be stable in cell growth media. The high surface charge absolute values could also explain observations in the AFM images that the particles are well dispersed on the surface with limited aggregation. The highly negative zeta-potential measured here is consistent with many other findings for fabricated nanoplastics [5] but it is unclear how this compares with environmentally recovered nanoplastics given the relative dearth of such measurements.

To further examine the stability of nanoplastics under different conditions, we used tangential flow filtration (TFF) as a scalable technique to concentrate the particles to varying levels and found minimal effects on particle size. For example, using DLS, we find consistent PSDs for the as-produced and tenfold concentrated PP dispersions, with mean particle sizes and corresponding PSD standard deviations of (269 nm, 163 nm) and (264 nm, 141 nm), respectively. We have also tested the long-term stability of the nanoplastic suspensions in different media over the course of two weeks. Using DLS, we have observed no substantial change in PSD in milli-Q water over time (see Fig. 3a). To determine the suitability of the nanoplastics for use in biological testing, we measured the stability of the suspensions in cell media; here, we use the same media for cell culture (DMEM supplemented with 10% FBS). Upon initial loading and using DLS to monitor the particle sizes, we find that particle diameter increases for all nanoplastics tested with the mean particle size and the corresponding standard deviation for PP, HDPE, and PET equal to (324 nm, 185 nm), (278 nm, 114 nm), and (265 nm, 167 nm), respectively. Importantly, we find that after the initial change in particle diameter, the PSDs remain stable over the course of two weeks (see Fig. 3b-d). This behavior is consistent with limited aggregation, possibly mediated by the formation of a protein corona around the particles, which increases object size while also enhancing stability in the new, high-salt molarity solution [50, 68, 69]. It should be noted that DLS is an excellent technique to monitor nanoparticle dispersion stability against aggregation since it is most sensitive to the largest particle within PSD.

For use as a reference material, the batch-to-batch variation during fabrication should be small and within a batch the material should be homogeneous. We find using intensity-weighted DLS for the PP samples that the mean particle size has a within batch standard deviation of 12 nm and between batch standard deviation of 12 nm when assessed across 10 different ampules and up to three independent replicates for each ampule. For HDPE the within batch and between batch standard deviations are 22 nm and 4.5 nm and for PET they are 8.8 nm and 29 nm when assessed across three independent replicates for each. Additionally, we found that the IR spectrum

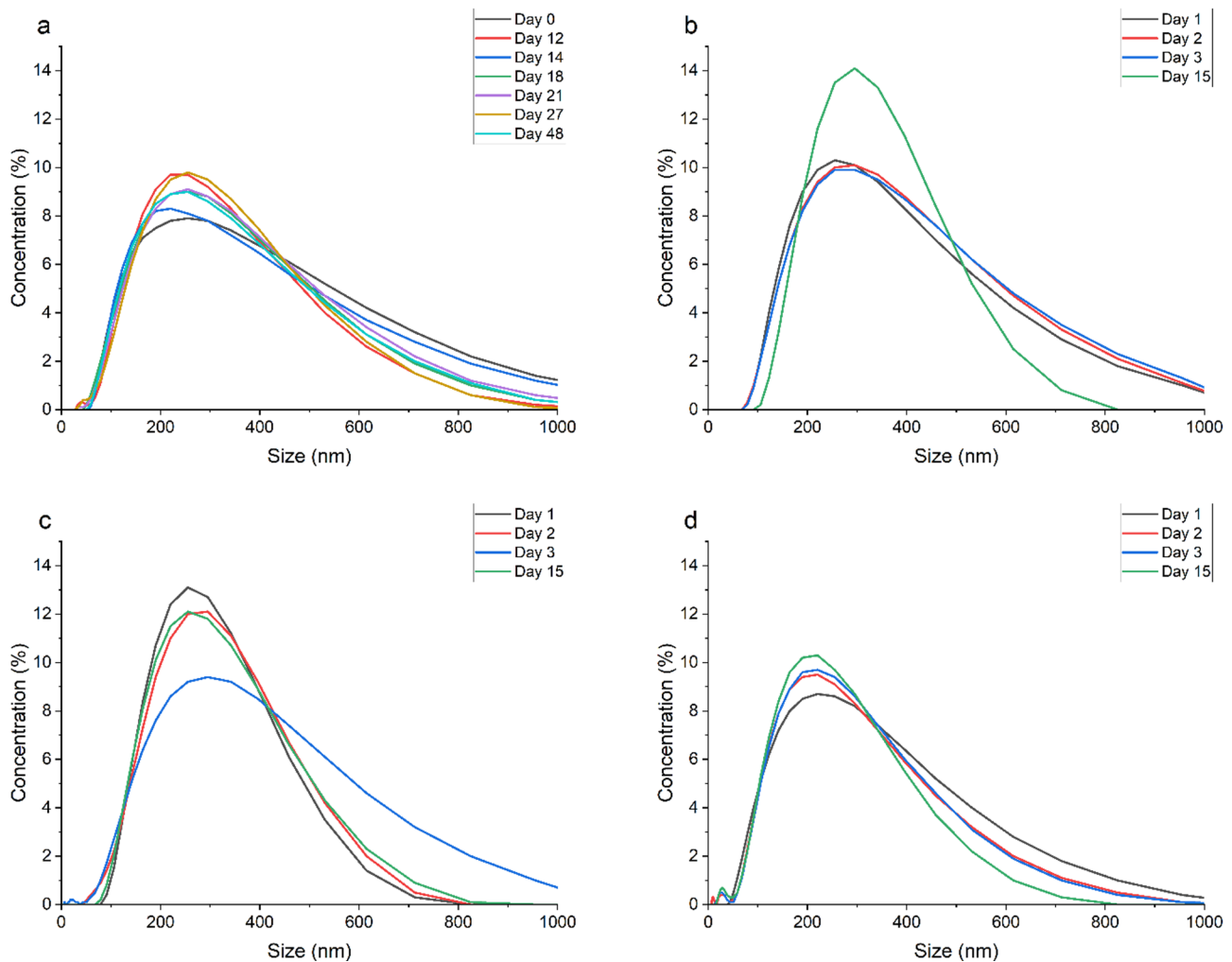


Fig. 3 Stability of nanoplastics in different media. **(a)** Intensity-weighted PSD of PP nanoplastics in water measured using DLS over the course of two months. **(b-d)** Nanoplastics are added to cell media and measured at day 1 (black), day 2 (red), day 3 (blue) and day 15 (green) with results reported using intensity-weighted PSD from DLS. **(b)** PSD of PP nanoplastics in media **(c)** PSD of HDPE nanoplastics in media **(d)** PSD of PET nanoplastics in media

from each batch was indistinguishable within the uncertainty of the measurement from the independent replicates.

Biological characterization: two-dimensional (2D) cell culture

The effects of MNPs on living organisms are a significant societal concern. After exposure to MNPs, there can be short-term effects, either due to the MNPs themselves or other additives and compounds they carry, and long-term effects due to their accumulation. Moreover, with long-term accumulation, there is the possibility of complex biological interactions leading to unexpected downstream effects that are not immediately apparent from simple cell models. To begin to address some of these issues and to assess the feasibility of the nanoplastics we produced for biological screening, we tested several different biological systems to measure the effects

of nanoplastic exposure. Here we first concentrated the suspension using TFF with a 10 kDa filter which simultaneously removes particles ≤ 2 nm in size. After concentration, the particles were resuspended at the appropriate concentration with no additional filtering. Future work will examine if particular size ranges are more or less biologically active.

As an initial screening test, cell viability after exposure to nanoplastics was measured using A549 human lung adenocarcinoma cells and THP-1 human macrophage cells using high concentrations of nanoplastics (1×10^{10} particles/mL and 1×10^{12} particles/mL). A549 is widely used as an alveolar epithelial (type II) cell line with well-documented metabolizing and barrier-related functions [70], while THP-1 is a monocyte that can be differentiated into macrophage like cells that can actively phagocytose foreign particulates and mount an immune response [71]. Both cell types are frequently used in nanoparticle

immunotoxicity assays, facilitating evaluation of phagocytosis, reactive oxygen species (ROS) generation, and cytokine release allowing comparative, high-throughput probing of uptake, viability, oxidative stress, and inflammation in epithelial and immune cells [72]. The concentrations of 1×10^{12} and 1×10^{10} particles/mL were chosen to represent high and moderate exposures that elicit measurable cellular responses without complete cytotoxicity and are not representative of what is commonly found in the environment. This is in alignment with commonly employed concentrations in nanoplastic cytotoxicity assessments [73]. In addition to laser ablated particles, we also performed an exposure test for commercially available spherical polystyrene (PS) nanoplastics, since these are widely used in nanotoxicology as a reference point due to their easy availability and uniformity and may serve as a common point of comparison for assessing plastic particle induced biological responses. Specifically, we treated cells with 1×10^{12} particles/mL of 50 nm PS and carboxylate groups functionalized PS particles. Consistent with previous findings [50, 74], we observed no significant effects on cell viability after treating the cells for 48 h with either laser ablated particles (Fig. 4a-b) or with the PS spheres (Supporting Figure S4a). Previous work, however, has shown that nanoplastics can induce elevated levels of intracellular and extracellular ROS that result in oxidative damage, impaired mitochondrial function and inflammation [75]. Here, we also find that nanoplastic exposure can lead to increased ROS levels in both THP-1 and A549 cells. For example, A549 cells treated with 1×10^{12} particles/mL of HDPE and PP for 48 h showed approximately a 3- and 6-fold increase in ROS levels compared to controls, respectively (Fig. 4c). Similarly, THP-1 cells under the same treatment showed 7- and 17-fold increases in ROS for HDPE and PP nanoplastics, respectively (Fig. 4e). Interestingly, neither PET nor PS nanoplastics significantly impacted ROS levels in either cell lines (Fig. 4c, e for PET, Supporting Figure S4b for PS). This is consistent with previous findings which also observed a minimal effect on cell viability and ROS generation using laser ablated PET to treat cells in 2D culture [50]. It has been observed that ROS levels can start to change from the homeostatic basal levels in cells within a few hours of appropriate stimulation [76]. Therefore, to evaluate the initiation of ROS production, a 6 h treatment with the highest concentration of 1×10^{12} particles/mL was conducted. The lower concentration was excluded because it did not elicit a significant ROS response compared to the controls (Fig. 4c, e). Interestingly, we find that at 6 h post-treatment, ROS levels are indeed higher than at 48 h post-treatment for both HDPE and PP exposure (Fig. 4c-e). A549 cells treated with HDPE and PP for 6 h experienced 14- and 17-fold increases in ROS levels, respectively (Fig. 4d). Similarly,

THP-1 cells treated with the laser-ablated nanoplastics for 6 h resulted in 22- and 29-fold increases in ROS levels for HDPE and PP, respectively (Fig. 4f). Similar to the 48 h treatment, no effect on ROS generation was observed with PET nanoplastic exposure (Fig. 4d, f) at 6 h.

Biological characterization: model organoid

Nanoplastic exposure in the environment can lead to long-term accumulation and affect an entire organ or organism [77, 78]. To evaluate the biological response of more complex tissues to nanoplastic exposure, we utilized a murine intestinal organoid system which has been previously demonstrated to have an intact lumen and can be used to help understand inflammatory responses in model tissues [79]. Organoids with enclosed lumens were employed to assess epithelial responses to external nanoplastic exposure. While this configuration does not directly replicate luminal uptake, it facilitates the study of barrier integrity, inflammatory responses and oxidative stress following basolateral or paracellular contact, which can occur in vivo when the epithelial barrier is compromised [80]. A murine model was selected due to its ready availability, reproducibility and suitability for mechanistic and in vivo correlation studies, with epithelial differentiation and stress-response pathways highly conserved with human intestine [81]. We treated the murine intestinal organoids with four different concentrations (1×10^{12} , 1×10^{10} , 1×10^8 , 1×10^6 particles/mL) of PP, HDPE and PET particles (Fig. 5a). After 5 days of exposure (day 7 in culture), organoids treated with the highest concentration of nanoplastics showed a shift in morphology, characterized by a predominance of smaller spheroidal structures compared to the controls, which maintained the typical budding architecture (Fig. 5b) indicating potential loss of viability. Viability assessment showed a significant loss of cell viability in the organoids treated with 1×10^{12} particles/mL concentration of PET nanoplastics. The organoids treated with the same concentration of HDPE and PP only showed a slight trend towards reduced viability (Fig. 5c), indicating that the impaired morphology may not be due to loss of viability. Similar to 2D cell cultures, treatment with PS50 ($97\% \pm 4\%$, $n = 3$) and PS50-COOH ($99\% \pm 7\%$, $n = 3$) showed no loss of viability in organoids. We also tested the organoids for evidence of increased levels of ROS. Exposure of gut epithelial cells to nanoplastics can activate NF- κ B, a key regulator of inflammation and oxidative stress. While this may not be directly fatal to cells, it can lead to subtle structural impairments [75, 82]. In order to assess the presence of ROS, the levels of H_2O_2 were quantified, which revealed significant upregulation of ROS levels in the organoids treated with the highest concentration of laser ablated nanoplastics, particularly in the case of HDPE (12-fold) and PP (23-fold) polymers (Fig. 5d). In

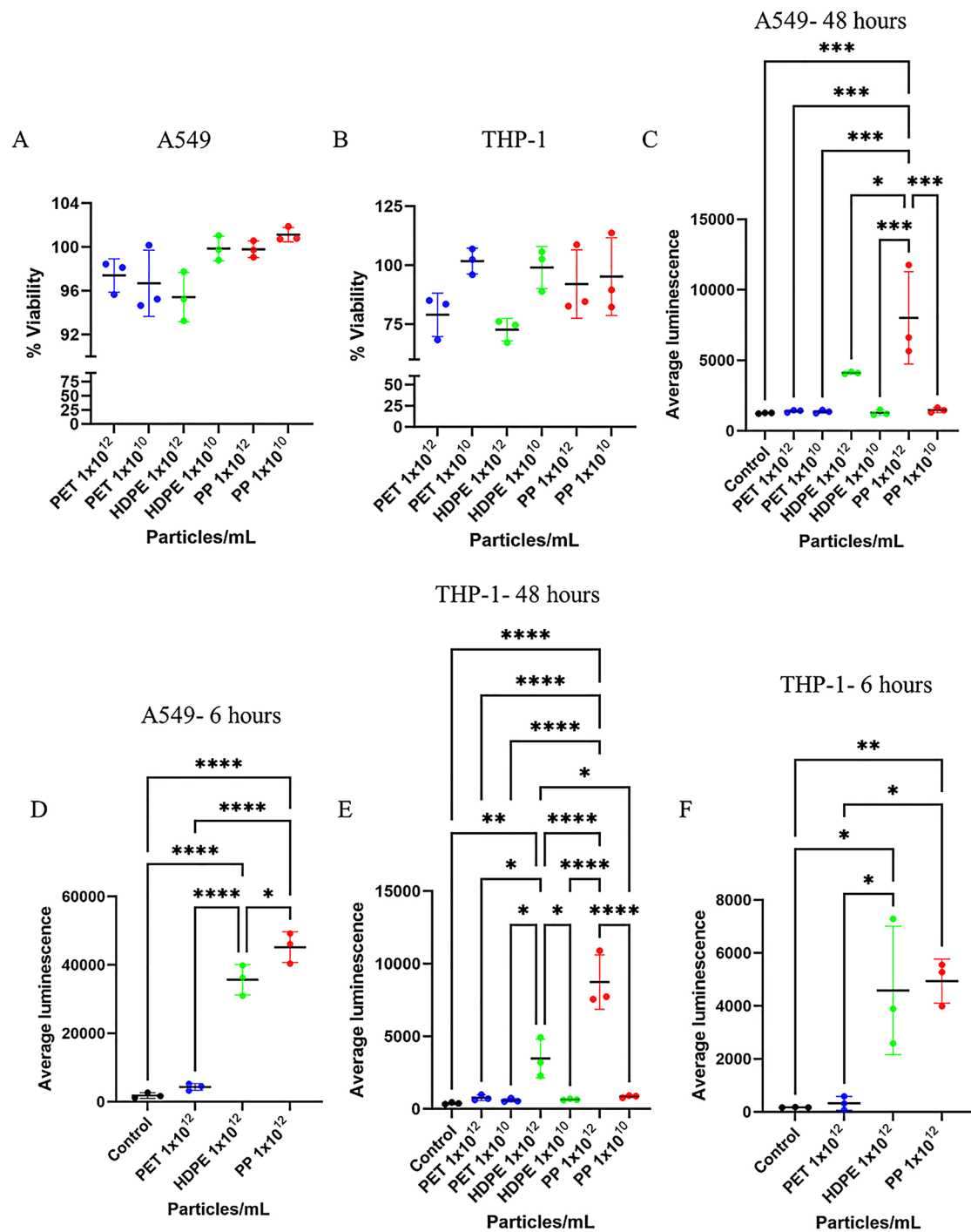


Fig. 4 Treatment of 2D cell cultures with laser ablated nanoplastics led to increased ROS generation without affecting cell viability. (a-b) Viability levels in (a) A549 and (b) THP-1 cells after 48-hour treatments. (c-f) Quantification of ROS levels in: (c) A549 cells after 48-hour treatment. (d) A549 cells after 6-hour treatment. (e) THP-1 cells after 48-hour treatment. (f) THP-1 cells after 6-hour treatment. Values on each graph are shown as mean \pm SD of three independent experiments ($n=3$). Statistical significance was determined with one-way ANOVA. $P < 0.05$ was considered significant. * $P < 0.05$; ** $P < 0.01$; *** $P < 0.001$; **** $P < 0.0001$. Only significant differences are shown in the graphs

contrast, exposure to PS50 at 1×10^{12} particles/mL did not elicit a ROS response, while carboxylated PS50 only showed a three-fold increase of ROS (Fig S4c) indicating that 3D organoids are likely more responsive since we did

not observe any elevated ROS response when 2D cells were treated with PS50-COOH (Fig S4b). To further validate these findings, the gene expression of *Sod1* (superoxide dismutase 1), an antioxidant enzyme that catalyzes

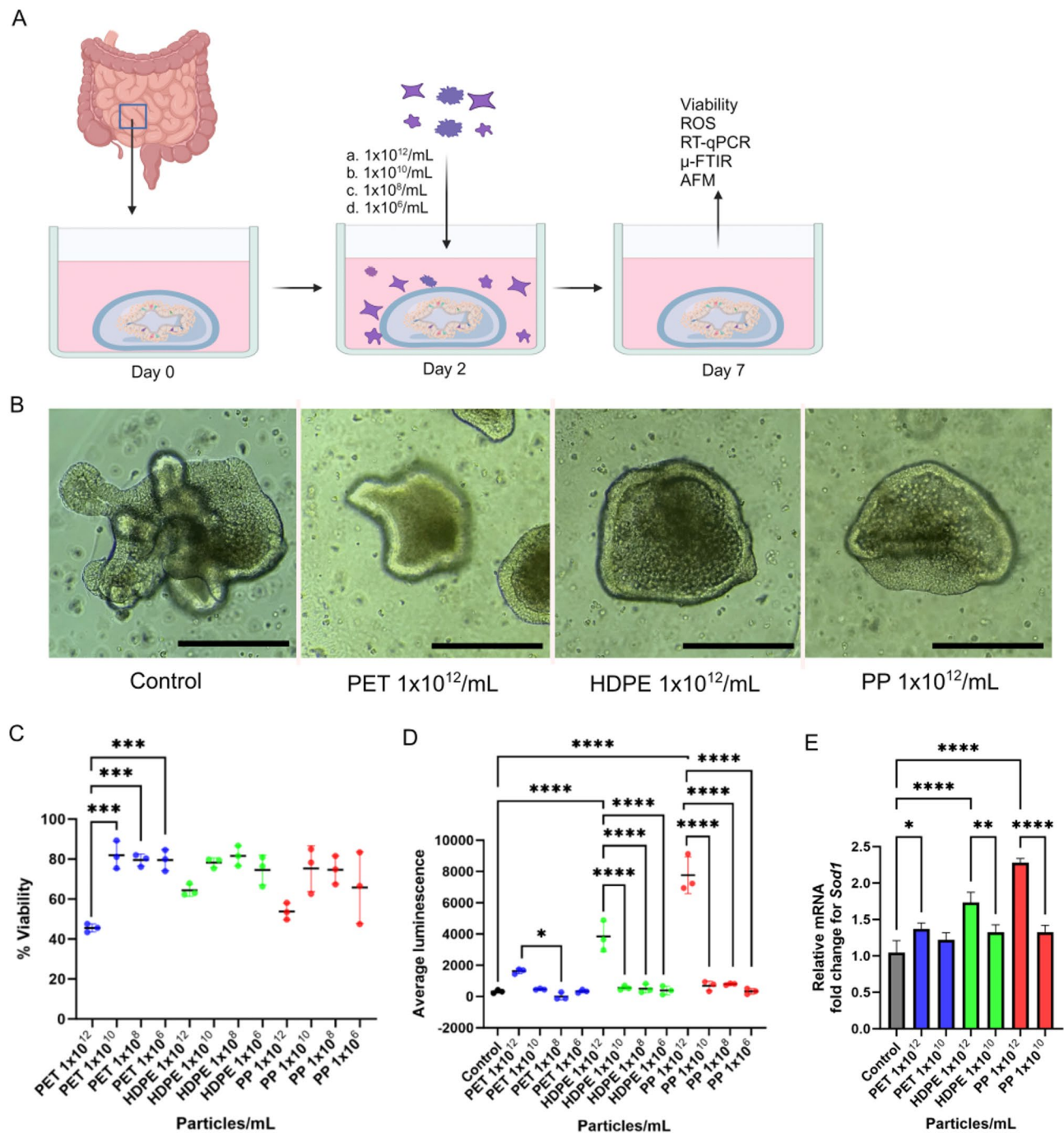


Fig. 5 Treatment with laser ablated nanoplastics upregulated ROS levels and genes involved in ROS regulatory enzymes. **(a)** Schematic representation of intestinal organoid generation and nanoplasic treatment. Generated using Biorender.com **(b)** Bright-field images of intestinal organoids after treatment with PET, HDPE and PP for 5 days. Scale bars measure $180 \mu\text{m}$. **(c)** Relative viability of organoids after 5 days of treatment. **(d)** Levels of ROS after 5 days of nanoplasic exposure. **(e)** Relative fold change of mRNA expression for *Sod1* enzyme. Values on each graph are shown as mean \pm SD of three independent experiments ($n=3$). Statistical significance was determined with one-way ANOVA. $P > 0.05$ was considered not significant. * $P < 0.05$; ** $P < 0.01$; *** $P < 0.001$; **** $P < 0.0001$

the conversion of superoxide radicals to maintain redox balance, was evaluated [83]. Since the ROS levels for the organoids treated with lower concentrations of 1×10^8 and 1×10^6 particles/mL were similar to the controls and

the ones treated with $1 \times 10^{10}/\text{mL}$; they were excluded from further analysis. Additionally, given the minimal apparent impact of PS50 and PS50-COOH exposure, they were also excluded from any further analysis. The

transcription of *Sod1* was found to be upregulated for all three laser-ablated polymers (Fig. 5e). This is in agreement with previous work, which has shown that exposure to plastic polymers leads to activation of antioxidant genes (e.g. *Sod1*) in zebrafish [84].

In the context of environmental toxicants such as nanoplastics, oxidative stress induced by excess ROS production plays a role in inflammatory response [75]. In addition to direct oxidative damage, ROS can serve as key mediators of NF- κ B leading to the secretion of pro-inflammatory cytokines such as TNF- α , IL-1 β (IL1B) and IL6 [85–87]. PP nanoparticulate can lead to elevated levels of ROS leading to induction of inflammatory factors TNF- α , IL1B and IL6 and increased instances of cytotoxicity in murine lungs and A549 cancer cells [87]. Similar to these findings, the laser ablated nanoplastics also led to the upregulation of inflammatory factors in the organoids at the highest tested concentration of 1×10^{12} particles/mL (Fig. 6a-c). Polymers HDPE and PP lead to increased transcription levels for both *Il1b* and *Il6* (Fig. 6a, c), while only PP nanoplastic treatments upregulated *Tnf* (Fig. 6b). Treatments with PET nanoplastics did not seem to significantly alter the expression of these inflammatory factors (Fig. 6a-c), which is unsurprising since PET treatment did not substantially affect ROS levels in either cell culture (Fig. 4c-f) or organoids. (Fig. 5d).

Biological characterization: organoid co-culture

The organoids used in the previous experiments that were derived via leveraging the *Lgr5* +ve intestinal stem cells do not contain any immune cells [88]. While utilizing these organoids provided critical insights into the

response mediated by the epithelial cells of the intestine, they failed to recapitulate the complex epithelial-immune interactions observed in vivo [88, 89]. Innate immune cells, such as macrophages and dendritic cells, play a key role in sensing and responding to environmental stressors such as nanoplastics [87, 90, 91]. THP1 monocytes/macrophages can mount an inflammatory response via the production of IL6 and IL8 when exposed to nanoscale PS nanoplastics [92] and we found they responded with significantly increased ROS levels in cell culture (Fig. 4d, f). Similarly, animal studies with murine models showed increased alveolar accumulation of immune cells (e.g. macrophages, neutrophils and lymphocytes), which resulted in nanoplastic internalizations and increased ROS and inflammation when treated with PP nanoplastics [87]. In order to recapitulate the interplay of epithelial and immune cells, we adopted a co-culture model using cell culture inserts, where a monolayer of all the different epithelial cells derived from intestinal organoids were cultured on one side of the porous insert, while murine macrophages (RAW264.7) were seeded on the opposite side [93] (Fig. 7a). This system allows mimicking the interaction between epithelial and basolateral immune cells through paracrine communication similar to intestinal microenvironment in vivo. In addition, this system allowed modeling luminal exposure of intestinal epithelial cells as nanoplastics were applied to the apical compartment to mimic luminal contact while maintaining polarized barrier function and immune communication across the interface [94].

The co-culture model elicited a higher ROS and inflammatory response for all three polymers when compared

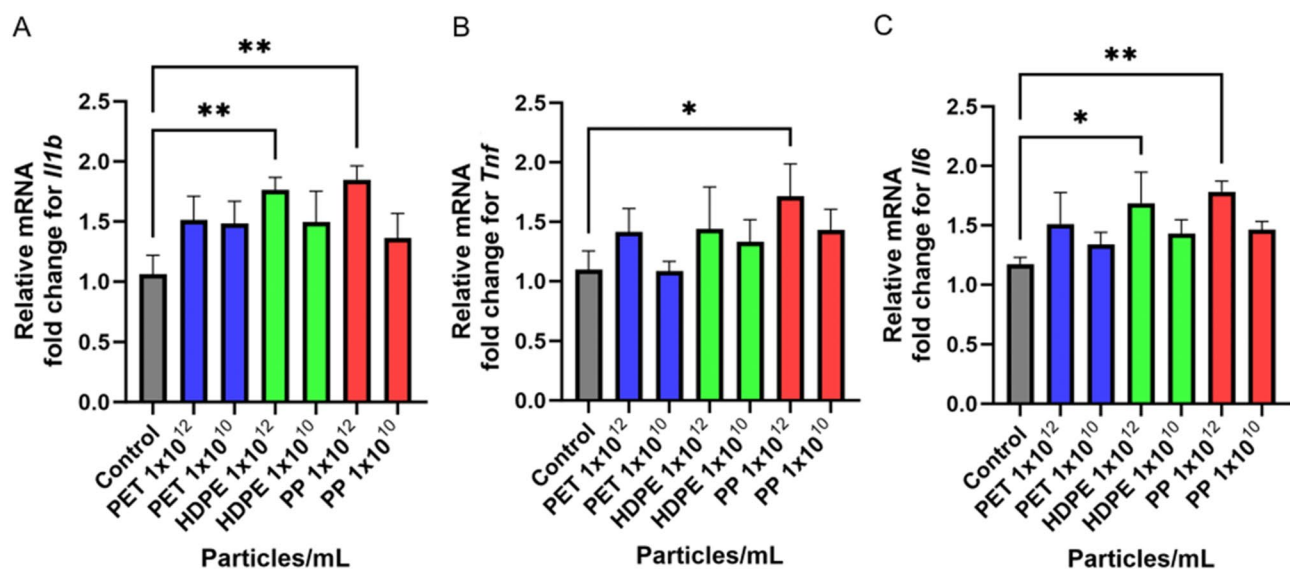


Fig. 6 Treatment with laser ablated nanoplastics induced inflammation in the intestinal organoids. (a-c) Relative fold change of mRNA expression for (a) *Il1b*, (b) *Tnf* and (c) and *Il6*. Values on each graph are shown as mean \pm SD of three independent experiments ($n = 3$). Statistical significance was determined with one-way ANOVA. $P > 0.05$ was considered not significant. * $P < 0.05$; ** $P < 0.01$; *** $P < 0.001$; **** $P < 0.0001$

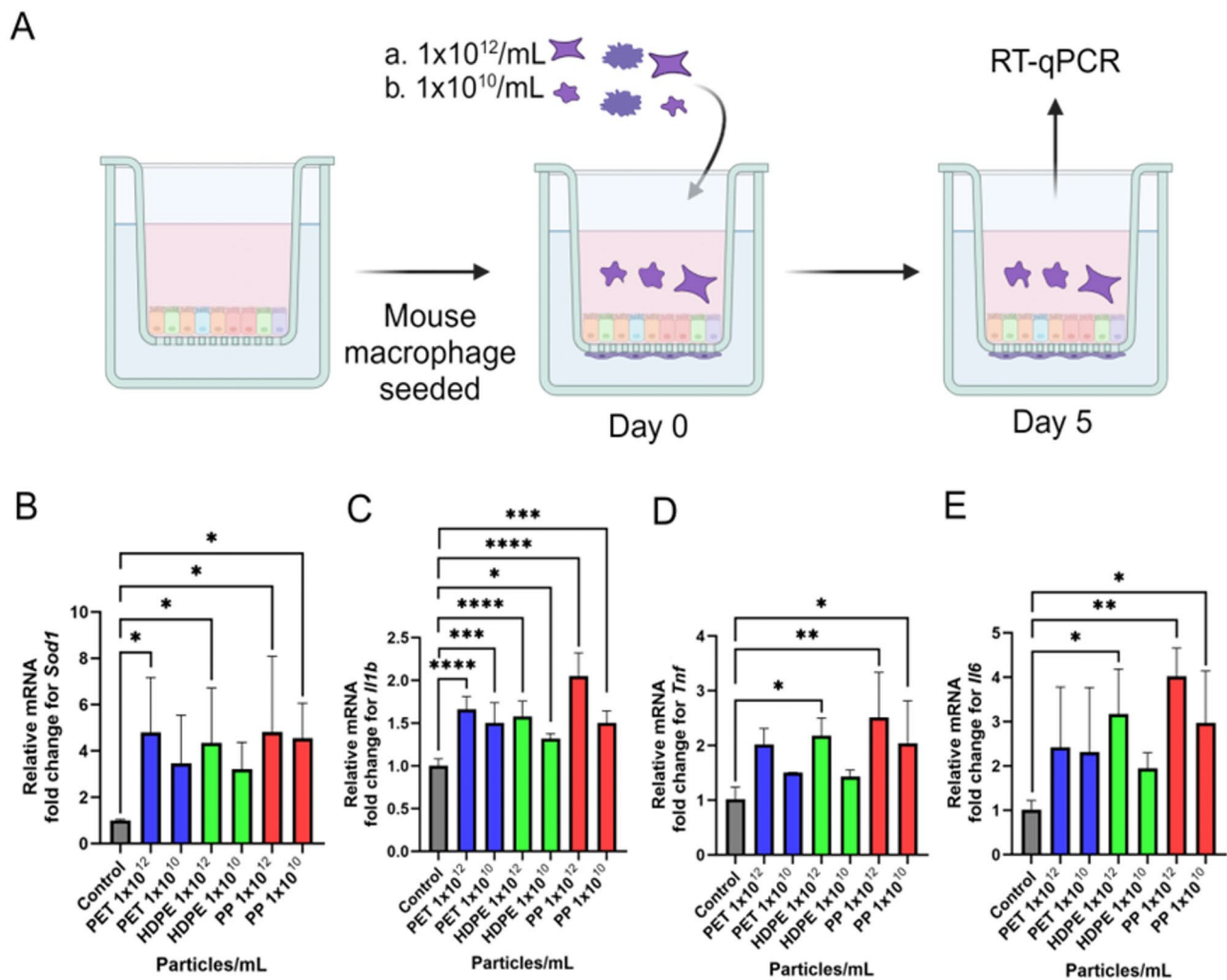


Fig. 7 Treatment of laser-ablated nanoplastics on a co-culture model with intestinal organoid and macrophages leads to greater levels of oxidative stress and inflammation. **(a)** Schematic representation of intestinal organoid and macrophage co-culture model generation and treatment. Generated using Biorender.com **(b-e)** Relative fold change of mRNA expression for **(b)** *Sod1*, **(c)** *Tnf*, **(d)** *Il1b* and **(e)** *Il6*. Values on each graph are shown as mean \pm SD of three independent experiments ($n=3$). Statistical significance was determined with one-way ANOVA. $P>0.05$ was considered not significant. $*P<0.05$; $**P<0.01$; $***P<0.001$; $****P<0.0001$

against organoids alone (Figs. 5e, 6a-c and 7b-e). Both *Tnf* and *Il6* expressions increased greater than two-fold when exposed to both concentrations of PP; while only the higher concentration (1×10^{12} particles/mL) elicited a significant cytokine response (Fig. 7d-e). In the case of *Il1b*, both concentrations of all three polymers resulted in significant upregulation of transcription (Fig. 7c). This elevated immune response is likely due to elevated ROS production as indicated by expression of *Sod1* (greater than 3-fold) (Fig. 7b). Nanoplastic mediated ROS production can be explained by two mechanisms: extracellular and intracellular. Photo oxidative weathering of nanoplastics can result in chemical alterations that can facilitate the formation of free radicals, which can interact with atmospheric oxygen to produce secondary polymer alkyl radicals [75, 95]. These extracellular radicals

could give rise to higher levels of ROS after endocytosis [96]. In addition, immune cells such as macrophages can identify nanoplastics as foreign particles and engulf them via endocytosis in an attempt to neutralize them [97–99]. During this process, ROS are generated in fairly high quantities as products of NADPH-oxidase or other enzymatic reactions in the form of superoxide and hydrogen peroxide, which can result in elevated levels of cytokine secretion. These intracellular ROS produced by macrophages, along with extracellular ROS introduced by the laser-ablated nanoplastics, likely account for the elevated levels of ROS in the co-culture model.

Discussion

To understand the effect plastic waste has on living creatures and the environment, it is necessary to have materials that mimic the plastics found in the environment. To this end, many previous works have demonstrated possible routes to establishing RMs for nanoplastics; [4–6] however, these materials are not currently widely available or accessible for performing comparisons. Ideally, these different approaches could be compared against each other and with materials recovered from the environment to better understand which features of MNPs are most prominent in affecting different living organisms. For example, PET nanoparticles have been previously created using nanosecond laser ablation and tested on living cells [50, 51]. Those particles were found to have a minimal effect on cell viability in 2D culture, but did change metabolomic markers. The previously created PET nanoparticles are similar in size to the ones we have fabricated here and seem to share other similar physical characteristics (highly negative zeta potential and increased oxygen content). Our findings that cell viability and ROS production for 2D cells in culture are minimally affected are also consistent with their findings [50]. It is harder to compare our findings that the PET nanoparticles do produce changes in organoid and co-culture models versus the findings by Margi et al. that metabolomics are altered in 2D cell culture [51].

It is also unclear how to compare our findings that PP and HDPE nanoparticles have a more pronounced effect on the biological systems we tested than PET nanoparticles. It is conceivable that UV nanosecond laser ablation could be used to create such nanoparticles. Still, the high temperatures involved and the inconsistent scaling of the laser power needed for ablation of different plastics make it challenging to predict the end product [100, 101]. By contrast, other approaches to RM production could allow for comparisons, although these are potentially fraught, given the wide range of outcomes observed depending on the cell type and particle manufacturing method used. To truly address these issues, candidate RMs must be made available to others so that fair comparisons can be performed. The nanoscale PP used in the present study is now available to others [55] and we expect the nanoscale HDPE and PET to likewise be made available in the future.

Conclusion

Microplastics and nanoplastics are of increasing societal concern, having been detected across nearly all environmental compartments worldwide. However, their detection and quantification remain challenging, often hindered by contamination from sampling tools and the complex matrices that obscure plastic-specific signals. These challenges are compounded by the tendency of

environmental plastics to associate with other materials that further mask their presence. While some studies have found an association between the presence of MNPs in the body and poor health outcomes, establishing any causative relationship remains elusive.

In this study, we developed a universal laser-based approach to fabricate nanoscale plastic RMs that reproduce the key chemical features of environmentally aged plastics. The materials exhibit discoidal shapes, remain stable over the long term in aqueous environments, and are readily suitable for biological assessments. Moreover, they elicit pro-inflammatory responses consistent with previous observations, supporting their utility as comparative standards for future studies. These results demonstrate the potential of such materials as realistic benchmark RMs for both analytical and toxicological studies. By providing reproducible and well-characterized mimics of environmental nanoplastics, this work lays the foundation for improving detection reliability, enabling cross-method comparability, and advancing understanding of the biological and environmental impacts of plastic exposure.

Materials and methods

Fabrication of nanoplastics

All nanoplastics were synthesized using the same apparatus. For laser ablation, a short-pulse laser with a pulse length of 200 fs, center wavelength of 1030 nm, average power of 1.4 W and repetition rate of 200 kHz (Carbide, Light Conversion, Lithuania) and mode size of 8 mm was used. The light was sent to a set of galvo mirrors (GVS012, Thorlabs, USA) and focused using a 110 mm telecentric lens (LSM05-BB, Thorlabs, USA). Under these conditions, the focal spot is approximately 25 μm , giving a peak intensity at the focus of $\sim 7 \text{ TW}/\text{cm}^2$. The total scan area was approximately 177 mm^2 . For machining, the focus was moved in a spiral pattern across the surface. The scan speed was set to ensure that each laser shot had $\sim 50\%$ spatial overlap with the previous one, allowing machining to occur at the edge of the multi-shot regime while minimizing heating. Plastic was secured inside a glass cuvette filled with Milli-Q water and the water was exchanged continuously with a 500 mL bath. The cuvette was mounted on a computer-controlled stage, moving along the optic axis of the telecentric lens. For the PP and HDPE, the stage was moved 12 μm every 60 min and for the PET, the stage was moved 12 μm every 30 min. A typical batch was collected over a period of 72 h with $\sim 140 \text{ mg}$ of PP removed, $\sim 110 \text{ mg}$ of HDPE removed, and $\sim 330 \text{ mg}$ of PET removed during that time period. After collection, the nanoplastic solution was then filtered through a 2.7 μm glass microfiber membrane (Whatman, 1823-047) to remove any large particles before further characterization. For cell culture

experiments, the suspensions were concentrated using TFF with a 10 kDa filter. After concentration, the particles were resuspended at the appropriate concentration with no additional filtering.

Commercial plastics

PP (PP30-SH-000155), HDPE (ET32-SH-000300) and PET (ES30-SH-000150) stock materials were acquired from Goodfellow.

50 nm polystyrene (PS50, Polysciences, 08691-10) and 50 nm polystyrene particles functionalized with carboxylate (PS50-COOH, Polysciences, 15913-10) were purchased and used without other alteration.

Infrared (IR) analysis

Attenuated total reflectance (ATR) Fourier-transform infrared spectroscopy (FTIR) spectroscopy on bulk plastics was performed using a Bruker Hyperion II FTIR microscope with a 20× ATR objective with a Ge ATR element. An adjustable aperture limits the spectral accumulation to an area of 30 $\mu\text{m} \times 30 \mu\text{m}$. FTIR measurements were performed from 600 cm^{-1} to 4000 cm^{-1} at a resolution of 4 cm^{-1} with a coaddition of 32 scans.

FTIR microscopy on nanoplastics was performed using a Bruker Hyperion II FTIR microscope, with a 15×/0.4 NA (or 36×/0.52 NA) objective and a liquid-nitrogen-cooled MCT detector. An adjustable aperture was used to limit the observed area to 50 $\mu\text{m} \times 50 \mu\text{m}$. FTIR measurements were performed from 600 cm^{-1} to 4000 cm^{-1} at a resolution of 4 cm^{-1} with a coaddition of 128 scans.

Dynamic light scattering (DLS)

Particle size and zeta potential (ZP) were characterized using Zetasizer Nano ZS (Malvern Panalytical, UK). Samples were measured at 25 °C. Typically three size measurements were conducted for each sample with 21 runs, each lasting 10 s. PSD were determined using default parameters and the general-purpose model.

Zeta Potential measurements were conducted using the DTS1070 folded capillary zeta cell with as produced dispersions. For each sample, 3 measurements with minimum 50 runs and no delay between measurements were performed. The measurements were analyzed using the general-purpose mode with the Smoluchowski approximation.

Nanoparticle tracking analysis (NTA)

Nanoparticle tracking analyses were conducted using NanoSightPro (Malvern Panalytical, UK) with samples diluted using Milli-Q water accordingly to observe between 10 and 100 particles per frame. For each measurement, 10 sequential videos were recorded with automatic camera settings. Final concentration

measurements were calculated taking into account dilution before measurement.

Atomic force microscopy (AFM)

AFM height/topography images were recorded using NanoWizard II BioAFM (JPK Instruments, Berlin, Germany) mounted on an Olympus IX81 inverted microscope. HQ: XSC-11/Al BS tips (Cantilever C, MikroMasch, CA, USA) with a typical spring constant of $\sim 7 \text{ N/m}$ and a resonance frequency of $\sim 155 \text{ kHz}$ were used for images captured with a JPK atomic force microscope. Samples for AFM were made by spin-coating 200 μL laser ablated dispersions onto freshly cleaved 1-inch by 1-inch squares of mica substrate at 1000 rpm for 60 s with a pre-incubation time of 10 min. The dispersion was concentrated to 10 times its initial level using a KrosFlo KR2i TFF system (Repligen) and then diluted three-fold for spin-coating. Following some preliminary scans of 50 μm by 50 μm for sample overview, multiple areas of 2.5 μm by 2.5 μm and 5.0 μm by 5.0 μm were recorded with a 1024 pixel \times 1024 pixel resolution and a scan rate of $\sim 1 \text{ Hz}$. Data were analyzed using Gwyddion.

Cell culture

Experimental cells were kept in liquid nitrogen prior to cell seeding. Human lung carcinoma epithelial cells (A549 cells) (ATCC, CRM-CCL-185) and human leukemia monocytic cells (THP-1 cells) (ATCC, TIB-202) and mouse macrophage (RAW 264.7, ATCC, TIB-71) were maintained in 2D monocultures. All the cells used in these experiments were between passage number 8 and 16. A549 and RAW 264.7 cells were cultured in DMEM media (36250, StemCell Technologies) with 10% FBS (A5209502, ThermoFisher Sci.) and 1% penicillin/streptomycin (P/S, 15140122, ThermoFisher Sci.). THP-1 cells were cultured using RPMI-1640 media (36750, StemCell Technologies) supplemented with 10% FBS and 0.05mM 2-mercaptoethanol (M3148, SigmaAldrich). When plated, THP-1 cells received 50 ng/mL of phorbol 12-myristate 13-acetate (PMA) to induce differentiation into macrophages [102]. All RPMI-1640 media changes and plastic treatments included the same PMA concentration.

Murine small intestinal organoid culture

Mouse small intestinal organoids (70931, StemCell Technologies) were cultured in Mouse IntestiCult™ growth media (06005, StemCell Technologies) as previously reported [79]. Briefly, around 200 mouse organoids were resuspended in 50 μL of cold Matrigel® Growth Factor Reduced Basement Membrane Matrix (356231, Corning) and dispensed at the center of a well of 24-well plate, which has been pre-warmed at 37 °C for at least 1 h. After 5 min at room temperature, the plate is transferred

and incubated upside down at 37 °C and 5% CO₂ in a tissue culture incubator. The well is then topped up with 500 µL of media and cultured for 4 days. Cultures were maintained at low passage numbers (< 10).

Murine organoid and macrophage co-culture

Intestinal organoids were cultured in Matrigel domes for 7 days and then dissociated in single cells using Gentle Cell Dissociation Reagent (100–1077, StemCell Technologies) and trypsin. These cells were resuspended in Human IntestiCult™ growth media (06010, StemCell Technologies) supplemented with 10 µM Y-27,632 (72308, StemCell Technologies) and seeded on Costar® 6.5 mm Transwell®, 0.4 µm Pore Polyester Membrane Inserts (38024, Stem Cell Technologies). Once the cells reached confluency, monolayers seeded on cell culture inserts were inverted and placed into an empty 12-well plate. A 20 µL suspension containing 100,000 RAW 264.7 cells was added onto the bottom surface of the inserts and allowed to adhere for 2 h at 37 °C in 5% CO₂. The inserts were then returned to their original position into a 24-well plate and cultured in Human IntestiCult™ growth media. For nanoplastic treatments of co-cultures, plastic solutions were added to the top/apical side of the cell culture inserts only.

Viability assessment

A549 and THP-1 cells were seeded on separate 96-well plates and cultured for 24 h at a concentration of 10,000 cells per well to allow adhesion. Then, all cells were treated with 1×10^{10} and 1×10^{12} particles/mL of PET, HDPE and PP at 37 °C. For PS50 and PS50-COOH, only the highest concentration of 1×10^{12} particles/mL was utilized. As the nanoplastics were suspended in water, the media for the control group received the same volume of MilliQ water as the highest concentration (1×10^{12} particles/mL) group.

For organoids, approximately 50 intestinal organoids were resuspended in 10 µL Matrigel dispensed into the center of each well of a 96-well plate and allowed to gel for 30 min at 37 °C. They were then treated with laser ablated nanoplastic solutions of 1×10^6 , 1×10^8 , 1×10^{10} and 1×10^{12} particles/mL concentration. For PS50 and PS50-COOH, only the highest concentration of 1×10^{12} particles/mL was utilized.

After 48 h of exposure, the media was replaced with FBS and plastic-free media (DMEM for A549 and RPMI-1640 for THP-1), and cell viability was determined using CellTiter-Glo assays (G9241, Promega) as per the manufacturer's instructions.

Measurement of reactive oxygen species (ROS) levels

The reactive oxygen species (ROS) levels were determined utilizing ROS-Glo H₂O₂ Assay (Promega, G8820).

Similar to the viability assays, A549 and THP-1 cells were seeded on 96-well plates for 24 h at concentrations of 10,000 cells per well, and organoids were seeded at a concentration of 50 organoids/well, then treated with nanoplastics for 6–48 h depending on the experiment. As per the ROS-Glo H₂O₂ Assay protocol, an H₂O₂ substrate was added during the last 6 h of incubation. This substrate was added using fresh cell line specific media without FBS and plastics to reduce background signals. The ROS assay process was conducted as per the manufacturer's instructions.

Reverse transcription quantitative polymerase chain reaction

Organoids and organoid-macrophage co-cultures were treated with 1×10^{10} and 1×10^{12} particles/mL of plastic solutions in 24-well plates. After 48 h of incubation, the organoids and co-culture monolayers were washed with phosphate buffered saline (PBS) before being lysed for RNA extraction. RNA was isolated using RNeasy Mini Kit (Qiagen, 74104) and RT-qPCR was carried out with Power SYBR Green RNA-to-CT 1-Step Kit (ThermoFisher Scientific, 4389986). The expression levels of *Sod1* (QT01762719, Qiagen), *Tnf* (QT00104006, Qiagen), *Il1b* (QT01048355, Qiagen) and *Il6* (QT00098875, Qiagen) genes were normalized to reference gene *Gapdh* (QT01658692, Qiagen). Relative expression was determined using the $\Delta\Delta C_t$ method. The statistical analysis was performed on ΔC_t values.

Statistical analysis for biological characterization

All the results described here are from at least three independent experiments. Data were analyzed using GraphPad Prism 8 software. A one-way analysis of variance (ANOVA) was conducted for more than two groups, followed by a post-hoc test and adjustment for multiple comparisons. A value of $p < 0.05$ was set as the limit of statistical significance.

Abbreviations

AFM	Atomic force microscopy
ATR	Attenuated total reflectance
DLS	Dynamic light scattering
FTIR	Fourier-transform IR
HDPE	High-density polyethylene
IR	Infrared
MNP	Micro and nanoplastic
NTA	Nanoparticle tracking analysis
PET	Polyethylene terephthalate
PP	Polypropylene
PSD	Particle size distribution
PS	Polystyrene
RM	Reference material
ROS	Reactive oxygen species
Sod1	Superoxide dismutase 1
TFF	Tangential flow filtration

Supplementary Information

The online version contains supplementary material available at <https://doi.org/10.1186/s43591-025-00157-2>.

Supplementary Material 1

Acknowledgements

The authors thank R. Lausten and D. Guay (NRC-QN) for their support.

Author contributions

A.F.P. fabricated the nanoplastics and analyzed the data. M.C. performed the AFM and TFF measurements. S.S. performed the cell measurements and analyzed the data. Z.J.J. analyzed the light scattering data. M.Z. performed the light scattering measurements and processed the samples. D.P. performed the IR measurements. A.S. and D.C. contributed to the fabrication setup design. M.V. contributed to the cell measurements. S.Z. oversaw the project. A.F.P., M.C. and S.Z. conceived of the project. A.F.P. wrote the manuscript with contributions from M.C., S.S., Z.J.J. and S.Z. All authors contributed to editing the manuscript.

Funding

The authors gratefully acknowledge the financial support provided by the Ocean Program at the National Research Council Canada (NRC) and the Government of Canada's Advancing a Circular Plastics Economy for Canada Program.

Data availability

Source data is available on the Canadian Ocean Microplastic Explorer (COMEX) platform (<https://modolo.ca/comex/data>).

Declarations

Competing interests

The authors declare no competing interests.

Received: 21 August 2025 / Accepted: 27 October 2025

Published online: 01 December 2025

References

- Allen D, Allen S, Abbasi S, Baker A, Bergmann M, Brahney J, et al. Microplastics and nanoplastics in the marine-atmosphere environment. *Nat Rev Earth Environ*. 2022 June;3(6):393–405.
- Evangelidou N, Grythe H, Klimont Z, Heyes C, Eckhardt S, Lopez-Aparicio S et al. Atmospheric transport is a major pathway of microplastics to remote regions. *Nat Commun*. 2020 July 14;11(1):3381.
- Thushari GGN, Senevirathna JDM. Plastic pollution in the marine environment. *Heliyon*. 2020;6(8):e04709.
- Sørensen L, Gerace MH, Booth AM. Small micro- and nanoplastic test and reference materials for research: current status and future needs. *Camb Prisms: Plast*. 2024;2:e13.
- Ducoli S, Kalčíková G, Velimirovic M, Depero LE, Federici S. Production, characterization, and toxicology of environmentally relevant nanoplastics: a review. *Environ Chem Lett*. 2025;23:649–75.
- Crosset-Perrotin G, Moraz A, Portela R, Alcolea-Rodriguez V, Burrueco-Subirà D, Smith C, et al. Production, labeling, and applications of micro- and nanoplastic reference and test materials. *Environ Science: Nano*. 2025;12(6):2911–64.
- Baby MG, Gerritse J, Beltran-Sanahuja A, Wolter H, Rohais S, Romero-Sarmiento MF. Aging of plastics and microplastics in the environment: a review on influencing factors, quantification methods, challenges, and future perspectives. *Environ Sci Pollut Res*. 2025;32(3):1009–42.
- Zhao J, Lan R, Wang Z, Su W, Song D, Xue R, et al. Microplastic fragmentation by rotifers in aquatic ecosystems contributes to global nanoplastic pollution. *Nat Nanotechnol*. 2024;19(3):406–14.
- ter Halle A, Ladirat L, Gendre X, Goudouneche D, Pusineri C, Routaboul C et al. Understanding the fragmentation pattern of marine plastic debris. *Environ Sci Technol*. 2016;50(11):5668–75.
- Ter Halle A, Jeanneau L, Martignac M, Jardé E, Pedrono B, Brach L, et al. Nanoplastic in the North Atlantic subtropical Gyre. *Environ Sci Technol*. 2017;51(23):13689–97.
- Wahl A, Le Juge C, Davranche M, El Hadri H, Grassl B, Reynaud S, et al. Nanoplastic occurrence in a soil amended with plastic debris. *Chemosphere*. 2021;262:127784.
- Andrady AL, Barnes PW, Bornman JF, Gouin T, Madronich S, White CC, et al. Oxidation and fragmentation of plastics in a changing environment; from UV-radiation to biological degradation. *Sci Total Environ*. 2022;851:158022.
- Liu S, Shi J, Wang J, Dai Y, Li H, Li J et al. Interactions between microplastics and heavy metals in aquatic environments: a Review. *Front Microbiol*. 2021;12:652520.
- Liu S, Huang J, Zhang W, Shi L, Yi K, Yu H, et al. Microplastics as a vehicle of heavy metals in aquatic environments: A review of adsorption factors, mechanisms, and biological effects. *J Environ Manag*. 2022;302:113995.
- Ivleva NP. Chemical analysis of microplastics and nanoplastics: Challenges, advanced Methods, and perspectives. *Chem Rev*. 2021;121(19):11886–936.
- Fang C, Luo Y, Naidu R. Microplastics and nanoplastics analysis: options, imaging, advancements and challenges. *Trends Anal Chem*. 2023;166:117158.
- Santos FA, Andre RS, Alvarenga AD, Alves ALMM, Correa DS. Micro- and nanoplastics in the environment: a comprehensive review on detection techniques. *Environ Sci: Nano*. 2025;12(7):3442–67.
- Khan A, Jia Z. Recent insights into uptake, toxicity, and molecular targets of microplastics and nanoplastics relevant to human health impacts. *iScience*. 2023;26(2):106061.
- Rose PK, Yadav S, Kataria N, Khoo KS. Microplastics and nanoplastics in the terrestrial food chain: Uptake, translocation, trophic transfer, ecotoxicology, and human health risk. *Trends Anal Chem*. 2023;167:117249.
- Sharma VK, Ma X, Lichtfouse E, Robert D. Nanoplastics are potentially more dangerous than microplastics. *Environ Chem Lett*. 2023;21(4):1933–6.
- da Costa JP. Micro- and nanoplastics in the environment: research and policy-making. *Curr Opin Environ Sci Health*. 2018;1:12–6.
- Mitrano DM, Wick P, Nowack B. Placing nanoplastics in the context of global plastic pollution. *Nat Nanotechnol*. 2021;16(5):491–500.
- Hartmann NB, Hüffer T, Thompson RC, Hassellöv M, Verschoor A, Daugaard AE, et al. Are we speaking the same language? Recommendations for a definition and categorization framework for plastic debris. *Environ Sci Technol*. 2019;53(3):1039–47.
- Gigault J, El Hadri H, Nguyen B, Grassl B, Rowenczyk L, Tufenkji N, et al. Nanoplastics are neither microplastics nor engineered nanoparticles. *Nat Nanotechnol*. 2021;16(5):501–7.
- Bermúdez JR, Swarzenski PW. A microplastic size classification scheme aligned with universal plankton survey methods. *MethodsX*. 2021;8:101516.
- EFSA Panel on Contaminants in the Food Chain (CONTAM). Presence of microplastics and nanoplastics in food, with particular focus on seafood. *EFSA J*. 2016;14(6):e04501.
- United States Food and Drug Administration. Considering Whether an FDA-Regulated Product Involves the Application of Nanotechnology. Department of Health and Human Services; 2019 [cited 2025 Feb 26]. Available from: <http://www.fda.gov/regulatory-information/search-fda-guidance-documents/considering-whether-fda-regulated-product-involves-application-nanotechnology>
- International Organization for Standardization. [cited 2025 Oct 16]. ISO 80004-1:2023. Available from: <https://www.iso.org/standard/79525.html>
- Health Canada. Policy Statement on Health Canada's Working Definition for Nanomaterial. 2011 [cited 2025 Oct 16]. Available from: <https://www.canada.ca/en/health-canada/services/science-research/reports-publications/nanomaterial/policy-statement-health-canada-working-definition.html>
- Gigault J, Halle A, ter, Baudrimont M, Pascal PY, Gauffre F, Phi TL, et al. Current opinion: what is a nanoplastic? *Environ Pollut*. 2018;235:1030–4.
- Allan J, Belz S, Hoeveler A, Hugus M, Okuda H, Patri A, et al. Regulatory landscape of nanotechnology and nanoplastics from a global perspective. *Regul Toxicol Pharmacol*. 2021;1:122:104885.
- Jakubowicz I, Enebro J, Yarahmadi N. Challenges in the search for nanoplastics in the environment—A critical review from the polymer science perspective. *Polym Test*. 2021;93:106953.
- Duncan TV, Khan SA, Patri AK, Wiggins S. Regulatory science perspective on the analysis of microplastics and nanoplastics in human food. *Anal Chem*. 2024;96(11):4343–58.
- Balakrishnan G, Déniel M, Nicolai T, Chassenieux C, Lagarde F. Towards more realistic reference microplastics and nanoplastics: Preparation of

- polyethylene micro/nanoparticles with a biosurfactant. *Environ Sci: Nano*. 2019;6(1):315–24.
35. Rodríguez-Hernández AG, Muñoz-Tabares JA, Aguilar-Guzmán JC, Vazquez-Duhalt R. A novel and simple method for polyethylene terephthalate (PET) nanoparticle production. *Environ Sci: Nano*. 2019;6(7):2031–6.
36. Tanaka K, Takahashi Y, Kuramochi H, Osako M, Tanaka S, Suzuki G. Preparation of nanoscale particles of five major polymers as potential standards for the study of nanoplastics. *Small*. 2021;17(49):2105781.
37. Merdy P, Delpy F, Bonneau A, Villain S, Iordachescu L, Vollertsen J, et al. Nanoplastic production procedure for scientific purposes: PP, PVC, PE-LD, PE-HD, and PS. *Heliyon*. 2023;9(8):e18387.
38. Pessoni L, Veclin C, Hadri HE, Cugnet C, Davranche M, Pierson-Wickmann AC et al. Soap and metal-free polystyrene latex particles as a nanoplastic model. *Environ Sci: Nano*. 2019;6(7):2253–8.
39. Pikuda O, Xu EG, Berk D, Tufenkji N. Toxicity assessments of Micro- and nanoplastics can be confounded by preservatives in commercial formulations. *Environ Sci Technol Lett*. 2019;6(1):21–5.
40. Lambert S, Wagner M. Characterisation of nanoplastics during the degradation of polystyrene. *Chemosphere*. 2016;145:265–8.
41. Lambert S, Wagner M. Formation of microscopic particles during the degradation of different polymers. *Chemosphere*. 2016;161:510–7.
42. Ekvall MT, Lundqvist M, Kelsiene E, Šileikis E, Gunnarsson SB, Cedervall T. Nanoplastics formed during the mechanical breakdown of daily-use polystyrene products. *Nanoscale Adv*. 2019;1(3):1055–61.
43. McColley CJ, Nason JA, Harper BJ, Harper SL. An assessment of methods used for the generation and characterization of cryomilled polystyrene micro- and nanoplastic particles. *Microplast Nanoplast*. 2023;3(1):20.
44. Parker LA, Höppener EM, van Amelrooij EF, Henke S, Kooter IM, Grigoriadi K, et al. Protocol for the production of micro- and nanoplastic test materials. *Microplast Nanoplast*. 2023;3(1):10.
45. El Hadri H, Gigault J, Maxit B, Grassl B, Reynaud S. Nanoplastic from mechanically degraded primary and secondary microplastics for environmental assessments. *NanoImpact*. 2020;17:100206.
46. Blanco F, Davranche M, Fumagalli F, Ceccone G, Gigault J. A reliable procedure to obtain environmentally relevant nanoplastic proxies. *Environ Sci: Nano*. 2021;8(11):3211–9.
47. Song YK, Hong SH, Eo S, Shim WJ. The fragmentation of nano- and microplastic particles from thermoplastics accelerated by simulated-sunlight-mediated photooxidation. *Environ Pollut*. 2022;311:119847.
48. Pfohl P, Wagner M, Meyer L, Domercq P, Praetorius A, Hüffer T, et al. Environmental degradation of microplastics: how to measure fragmentation rates to secondary Micro- and nanoplastic fragments and dissociation into dissolved organics. *Environ Sci Technol*. 2022;56(16):11323–34.
49. Leng Y, Chen M, Cao X, Zou S. Laboratory simulated aging of polystyrene particles and characterization of the resulting nanoscale plastics. *J Environ Chem Eng*. 2023;11(5):110967.
50. Magri D, Sánchez-Moreno P, Caputo G, Gatto F, Veronesi M, Bardi G, et al. Laser ablation as a versatile tool to mimic polyethylene terephthalate nanoplastic pollutants: characterization and toxicology assessment. *ACS Nano*. 2018;12(8):7690–700.
51. Magri D, Veronesi M, Sánchez-Moreno P, Tolardo V, Bandiera T, Pompa PP, et al. PET nanoplastics interactions with water contaminants and their impact on human cells. *Environ Pollut*. 2021;271:116262.
52. Shirk MD, Molian PA. A review of ultrashort pulsed laser ablation of materials. *J Laser Appl*. 1998;10(1):18–28.
53. Balling P, Schou J. Femtosecond-laser ablation dynamics of dielectrics: basics and applications for thin films. *Rep Prog Phys*. 2013;76(3):036502.
54. Mirza I, Bulgakova NM, Tomáščík J, Michálek V, Haderka O, Fekete L, et al. Ultrashort pulse laser ablation of dielectrics: Thresholds, mechanisms, role of breakdown. *Sci Rep*. 2016;6(1):39133.
55. National Research Council of Canada. NPPP-1: Nanoscale Polypropylene Reference Material - NRC Digital Repository. 2025 [cited 2025 Oct 13]. Available from: <https://doi.org/10.4224/crm.2025.nppp-1>
56. Menzel T, Meides N, Mauel A, Mansfeld U, Kretschmer W, Kuhn M, et al. Degradation of low-density polyethylene to nanoplastic particles by accelerated weathering. *Sci Total Environ*. 2022;20:826:154035.
57. De Frond H, Rubinovitz R, Rochman CM. μ ATR-FTIR spectral libraries of plastic particles (FLOPP and FLOPP-e) for the analysis of microplastics. *Anal Chem*. 2021;93(48):15878–85.
58. Rajakumar K, Sarasvathy V, Thamarai Chelvan A, Chitra R, Vijayakumar CT. Natural weathering studies of polypropylene. *J Polym Environ*. 2009;17(3):191–202.
59. Syranidou E, Karkanorachaki K, Barouta D, Papadaki E, Moschovas D, Avgeropoulos A, et al. Relationship between the carbonyl index (CI) and fragmentation of polyolefin plastics during aging. *Environ Sci Technol*. 2023;57(21):8130–8.
60. Ioakeimidis C, Fotopoulou KN, Karapanagioti HK, Geraga M, Zeri C, Papanassiou E, et al. The degradation potential of PET bottles in the marine environment: an ATR-FTIR based approach. *Sci Rep*. 2016;6(1):23501.
61. Sang T, Wallis CJ, Hill G, Britovsek GJP. Polyethylene terephthalate degradation under natural and accelerated weathering conditions. *Eur Polym J*. 2020;136:109873.
62. Miranda MN, Sampaio MJ, Tavares PB, Silva AMT, Pereira MFR. Aging assessment of microplastics (LDPE, PET and uPVC) under urban environment stressors. *Sci Total Environ*. 2021;796:148914.
63. Boyd RD, Pichaimuthu SK, Cuenat A. New approach to inter-technique comparisons for nanoparticle size measurements; using atomic force microscopy, nanoparticle tracking analysis and dynamic light scattering. *Colloids Surf A*. 2011;387(1):35–42.
64. Bell NC, Minelli C, Tompkins J, Stevens MM, Shard AG. Emerging techniques for submicrometer particle sizing applied to Stöber silica. *Langmuir*. 2012;28(29):10860–72.
65. Filipe V, Hawe A, Jiskoot W. Critical evaluation of nanoparticle tracking analysis (NTA) by nanosight for the measurement of nanoparticles and protein aggregates. *Pharm Res*. 2010;27(5):796–810.
66. Kim A, Ng WB, Bernt W, Cho NJ. Validation of size Estimation of nanoparticle tracking analysis on polydisperse macromolecule assembly. *Sci Rep*. 2019;9(1):2639.
67. Patty PJ, Frisken BJ. Direct determination of the number-weighted mean radius and polydispersity from dynamic light-scattering data. *Appl Opt*. 2006;45(10):2209–16.
68. Ducoli S, Federici S, Nicsanu R, Zendrini A, Marchesi C, Paolini L, et al. A different protein Corona cloaks true-to-life nanoplastics with respect to synthetic polystyrene nanobeads. *Environ Sci: Nano*. 2022;9(4):1414–26.
69. Gopinath PM, Twayana KS, Ravanan P, John Thomas, Mukherjee A, Jenkins DF, et al. Prospects on the nano-plastic particles internalization and induction of cellular response in human keratinocytes. *Part Fibre Toxicol*. 2021;8(1):35.
70. Swain RJ, Kemp SJ, Goldstraw P, Tetley TD, Stevens MM. Assessment of cell line models of primary human cells by Raman spectral phenotyping. *Biophys J*. 2010;98(8):1703–11.
71. Holownia A, Niechoda A, Lachowicz J, Golabiewska E, Baranowska U. Phagocytosis and autophagy in THP-1 cells exposed to urban dust: possible role of LC3-associated phagocytosis and canonical autophagy. In: Pokorski M, editor. *Advances in Medicine and Medical Research*. Cham: Springer International Publishing; 2019 [cited 2025 Oct 16]. pp. 55–63. Available from: https://doi.org/10.1007/5584_2018_323
72. Peivandi Z, Shirazi FH, Teimourian S, Farnam G, Babaei V, Mehrparvar N, et al. Silica nanoparticles-induced cytotoxicity and genotoxicity in A549 cell lines. *Sci Rep*. 2024;24(1):14484.
73. Schröter L, Ventura N. Nanoplastic toxicity: insights and challenges from experimental model systems. *Small*. 2022;18(31):2201680.
74. Marcellus KA, Prescott D, Scur M, Ross N, Gill SS. Exposure of polystyrene Nano- and microplastics in increasingly complex in vitro intestinal cell models. *Nanomaterials*. 2025;15(4):267.
75. Hu M, Pallíć D. Micro- and nano-plastics activation of oxidative and inflammatory adverse outcome pathways. *Redox Biol*. 2020;37:101620.
76. Rodrigues M, Turner O, Stolz D, Griffith LG, Wells A. Production of reactive oxygen species by multipotent stromal cells/Mesenchymal stem cells upon exposure to Fas ligand. *Cell Transpl*. 2012;21(10):2171–87.
77. Jeong A, Park SJ, Lee EJ, Kim KW. Nanoplastics exacerbate parkinson's disease symptoms in *C. elegans* and human cells. *J Hazard Mater*. 2024;465:133289.
78. Nihart AJ, Garcia MA, El Hayek E, Liu R, Olewine M, Kingston JD, et al. Bioaccumulation of microplastics in decedent human brains. *Nat Med*. 2025;31(4):1114–9.
79. Sakib S, Zou S. Attenuation of chronic inflammation in intestinal organoids with graphene Oxide-Mediated tumor necrosis Factor- α Small interfering RNA delivery. *Langmuir*. 2024;40(7):3402–13.
80. Lehner R, Weder C, Petri-Fink A, Rothen-Rutishauser B. Emergence of nanoplastic in the environment and possible impact on human health. *Environ Sci Technol*. 2019;53(4):1748–65.
81. Foulke-Abel J, In J, Yin J, Zachos NC, Kovbasnjuk O, Estes MK, et al. Human enteroids as a model of upper small intestinal ion transport physiology and pathophysiology. *Gastroenterology*. 2016;150(3):638–e6498.

82. Covello C, Di Vincenzo F, Cammarota G, Pizzoferrato M. Micro(nano)plastics and their potential impact on human gut health: A narrative review. *Curr Issues Mol Biol.* 2024;46(3):2658–77.
83. Sheng Y, Abreu IA, Cabelli DE, Maroney MJ, Miller AF, Teixeira M, et al. Superoxide dismutases and superoxide reductases. *Chem Rev.* 2014;114(7):3854–918.
84. Santos D, Luzio A, Félix L, Cabecinha E, Bellas J, Monteiro SM. Microplastics and copper induce apoptosis, alter neurocircuits, and cause behavioral changes in zebrafish (*Danio rerio*) brain. *Ecotoxicol Environ Saf.* 2022;242:113926.
85. Lingappan K. NF- κ B in oxidative stress. *Curr Opin Toxicol.* 2018;7:81–6.
86. Didion SP. Cellular and oxidative mechanisms associated with Interleukin-6 signaling in the vasculature. *Int J Mol Sci.* 2017;18(12):2563.
87. Woo JH, Seo HJ, Lee JY, Lee I, Jeon K, Kim B, et al. Polypropylene nanoplastic exposure leads to lung inflammation through p38-mediated NF- κ B pathway due to mitochondrial damage. *Part Fibre Toxicol.* 2023;20(1):2.
88. Angus HCK, Butt AG, Schultz M, Kemp RA. Intestinal organoids as a tool for inflammatory bowel disease research. *Front Med.* 2020;6:2019.
89. Kromann EH, Cearra AP, Neves JF. Organoids as a tool to study homeostatic and pathological immune–epithelial interactions in the gut. *Clin Exp Immunol.* 2024;218(1):28–39.
90. Weber A, Schwiebs A, Solhaug H, Stenvik J, Nilsen AM, Wagner M, et al. Nanoplastics affect the inflammatory cytokine release by primary human monocytes and dendritic cells. *Environ Int.* 2022;163:107173.
91. Paget V, Dekali S, Kortulewski T, Grall R, Gamez C, Blazy K, et al. Specific uptake and genotoxicity induced by polystyrene nanobeads with distinct surface chemistry on human lung epithelial cells and macrophages. *PLoS ONE.* 2015;10(4):e0123297.
92. Prietl B, Meindl C, Roblegg E, Pieber TR, Lanzer G, Fröhlich E. Nano-sized and micro-sized polystyrene particles affect phagocyte function. *Cell Biol Toxicol.* 2014;30(1):1–16.
93. Noel G, Baetz NW, Staab JF, Donowitz M, Kovbasnjuk O, Pasetti MF, et al. A primary human macrophage-enteroid co-culture model to investigate mucosal gut physiology and host-pathogen interactions. *Sci Rep.* 2017;7(1):45270.
94. Kozuka K, He Y, Koo-McCoy S, Kumaraswamy P, Nie B, Shaw K, et al. Development and characterization of a human and mouse intestinal epithelial cell monolayer platform. *Stem Cell Rep.* 2017;9(6):1976–90.
95. Yousif E, Haddad R. Photodegradation and photostabilization of polymers, especially polystyrene: review. *SpringerPlus.* 2013;2(1):398.
96. Pannetier P, Cachot J, Clérandeau C, Faure F, Van Arkel K, de Alencastro LF, et al. Toxicity assessment of pollutants sorbed on environmental sample microplastics collected on beaches: part I-adverse effects on fish cell line. *Environ Pollut.* 2019;248:1088–97.
97. Geys J, Coenegrachts L, Vercammen J, Engelborghs Y, Nemmar A, Nemery B, et al. In vitro study of the pulmonary translocation of nanoparticles: A preliminary study. *Toxicol Lett.* 2006;160(3):218–26.
98. von Moos N, Burkhardt-Holm P, Köhler A. Uptake and effects of microplastics on cells and tissue of the blue mussel *mytilus Edulis L.* after an experimental exposure. *Environ Sci Technol.* 2012;46(20):11327–35.
99. Greven AC, Merk T, Karagöz F, Mohr K, Klapper M, Jovanović B, et al. Polycarbonate and polystyrene nanoplastic particles act as stressors to the innate immune system of Fathead minnow (*Pimephales promelas*). *Environ Toxicol Chem.* 2016;35(12):3093–100.
100. Elaboudi I, Lazare S, Belin C, Talaga D, Labrugère C. Underwater excimer laser ablation of polymers. *Appl Phys A.* 2008;92(4):743–8.
101. Elaboudi I, Lazare S, Belin C, Bruneel JL, Servant L. Organic nanoparticles suspensions preparation by underwater excimer laser ablation of polycarbonate. *Appl Surf Sci.* 2007;253(19):7835–9.
102. Hassan EM, Walker GC, Wang C, Zou S. Anti-leukemia effect associated with down-regulated CD47 and up-regulated calreticulin by stimulated macrophages in co-culture. *Cancer Immunol Immunother.* 2021;70(3):787–801.

Publisher's note

Springer Nature remains neutral with regard to jurisdictional claims in published maps and institutional affiliations.